Supplement

Figure S1. Injected current histograms. The number after the symbol "#" denotes the number of datasets, while the one after "n", the total number of injected current measurements for each site. SCH has an especially low number of dataset taken into account in the histogram as the measurements conducted with the Geotom instrument are not plotted, as for instrument-related reasons the injected currents between Geotom and SYSCAL cannot be compared. The Injected current intensities span over a wide range of values, from 0.01 to 100 mA. STO and MCO have the highest proportion of low injected current (<0.1 mA) also corresponding to high contact resistances, while SCH and CER have an insignificant proportion of low injected current (<0.1 mA). SCH has the narrower range of electrical current values. Narrower current distribution is the consequence of more homogeneous surface conditions and often better data quality, while low current injections lead to high contact resistances, more outliers, larger heterogeneity and often smaller data quality. The homogeneity is largest for the bedrock sites and smallest for the coarse-blocky terrain sites.
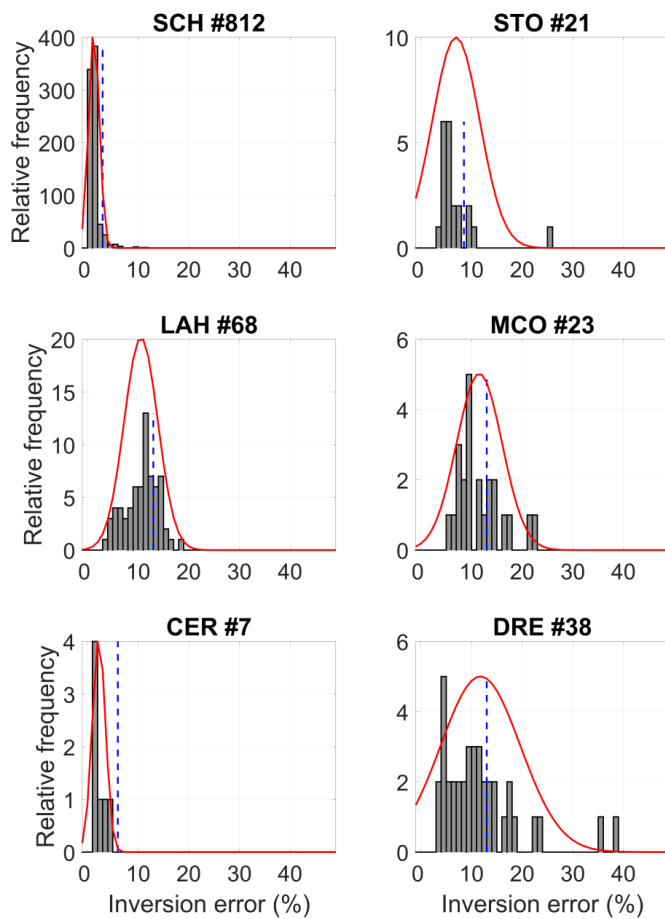
Figure S2. Inversion error histograms with a Gaussian fit (in red) and the empirical threshold (dashed blue lines) for each site. It shows the large variability of inversion error from one site to another, i.e. differences in data quality. A standard histogram analysis can only be conducted as the number of bins is not representative, i.e. too small. The number after the symbol "#" denotes the number of inverted datasets taken into account in the graph for each site.
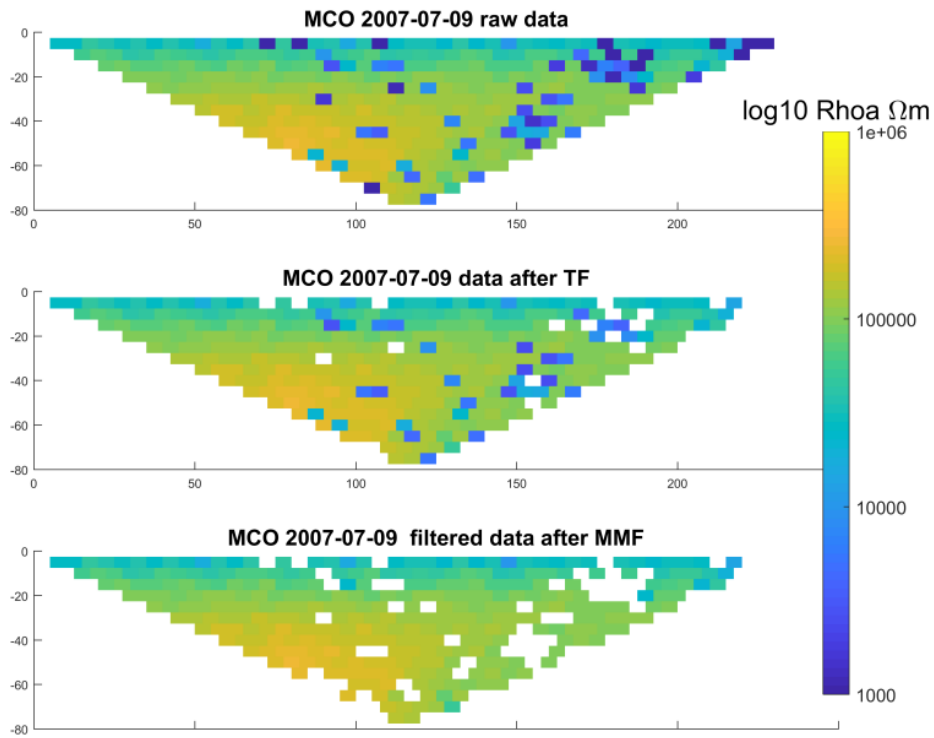
Figure S3. Example of the impact of the apparent resistivity filtering (step 1) on the pseudosections a) of raw data; b) after the systematic filter (SF) and c) after moving median filter (MMF) applied twice iteratively to remove outliers prior the inversion.
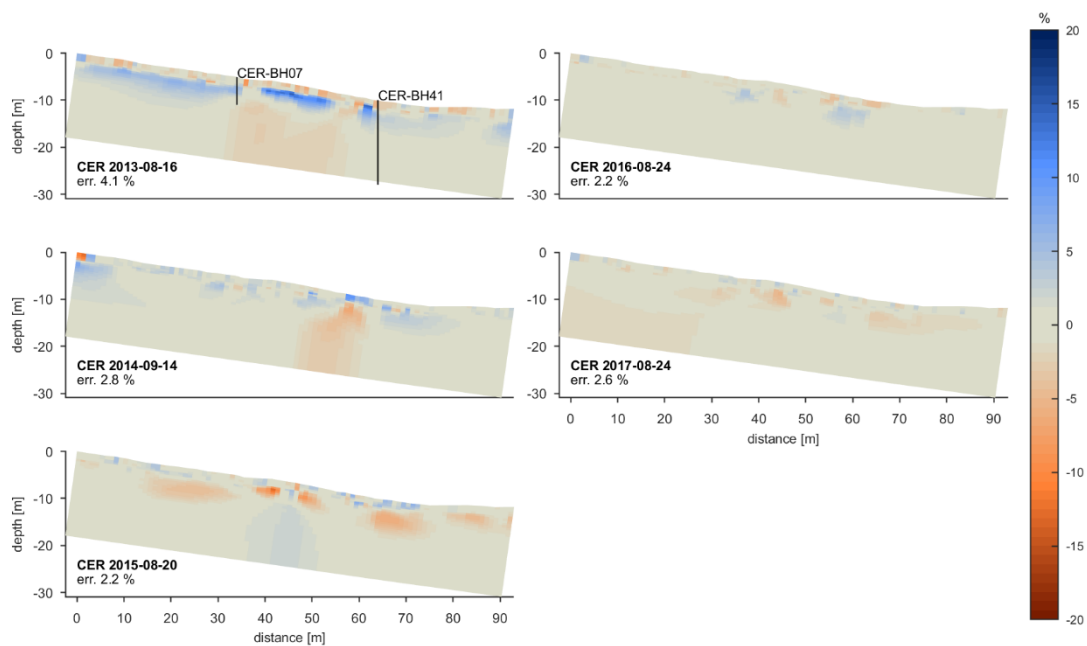
Figure S4. Percentage change of resistivity logarithm from the long-term median at CER monitoring site. The lowest resistivity values were measured in year 2015 at the end of summer. This time series is for the moment too short to detect any clear trend.
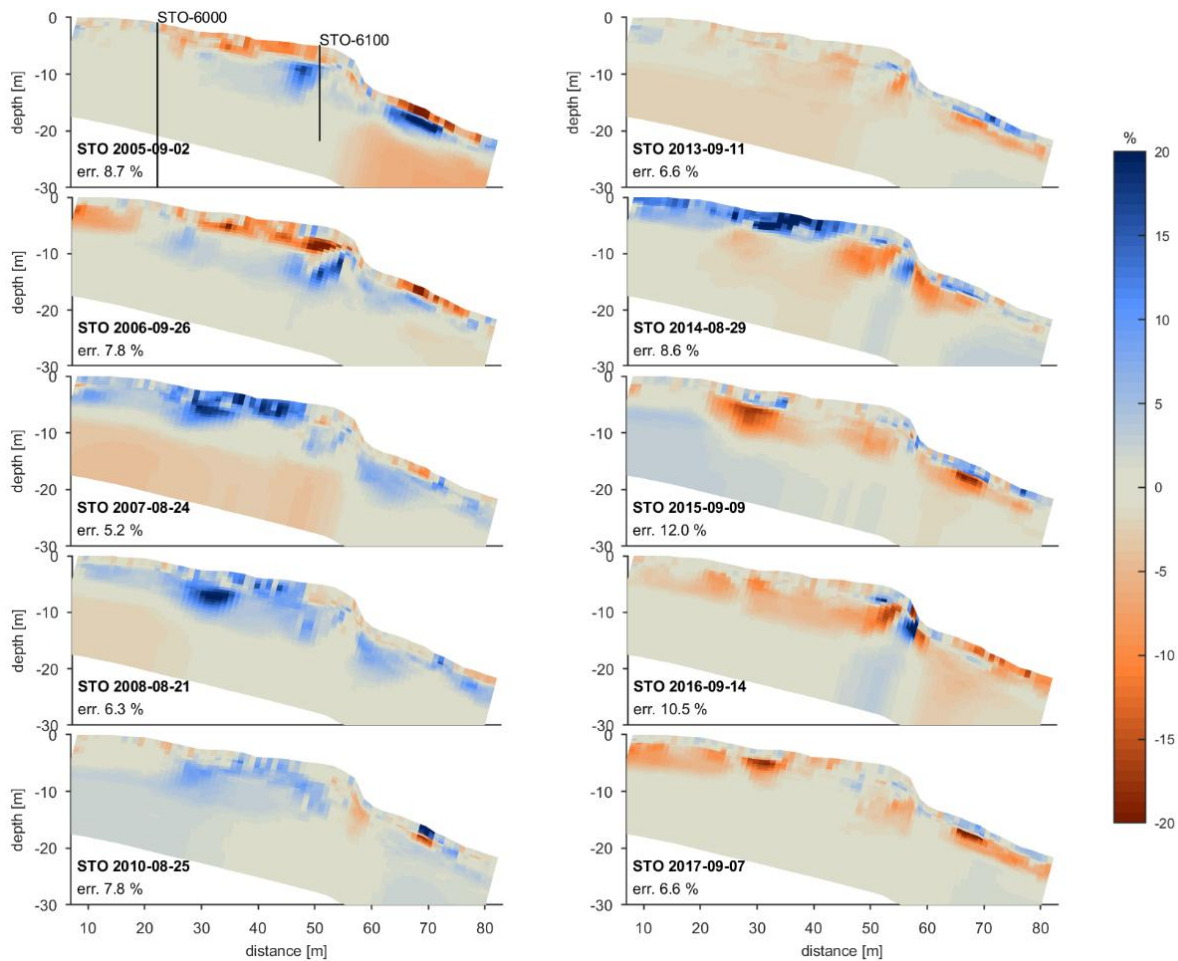
Figure S5. Percentage change of resistivity logarithm from the long-term median at STO monitoring site. Years 2006 and 2011 are omitted as they were conducted earlier in the season and therefore not comparable. The largest resistivity decrease occurs between 4 to 8 m depth, proving the increase in liquid water content within the upper part of the permafrost layer, i.e. permafrost degradation
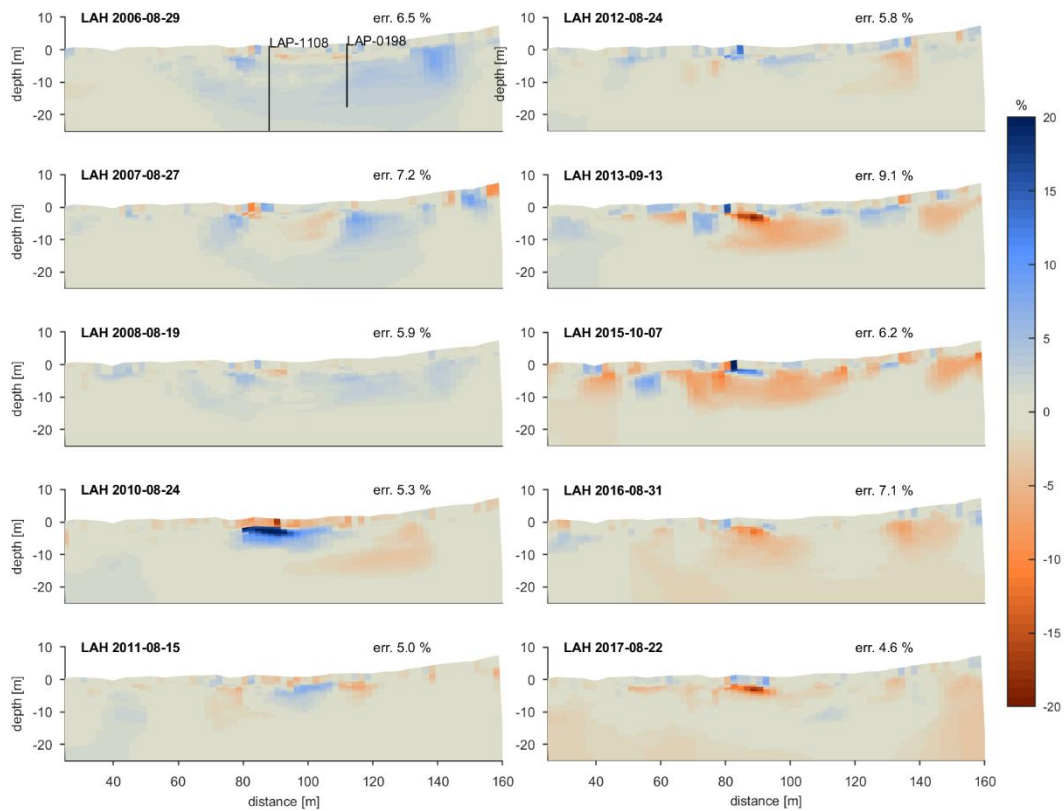
Figure S6. Percentage change of resistivity logarithm from the long-term median at LAH monitoring site. At depth between 5 and 20 m in the middle and right part of the tomogram (where permafrost occurs), the resistivities have a decreasing trend, i.e. water content increase and permafrost degradation.
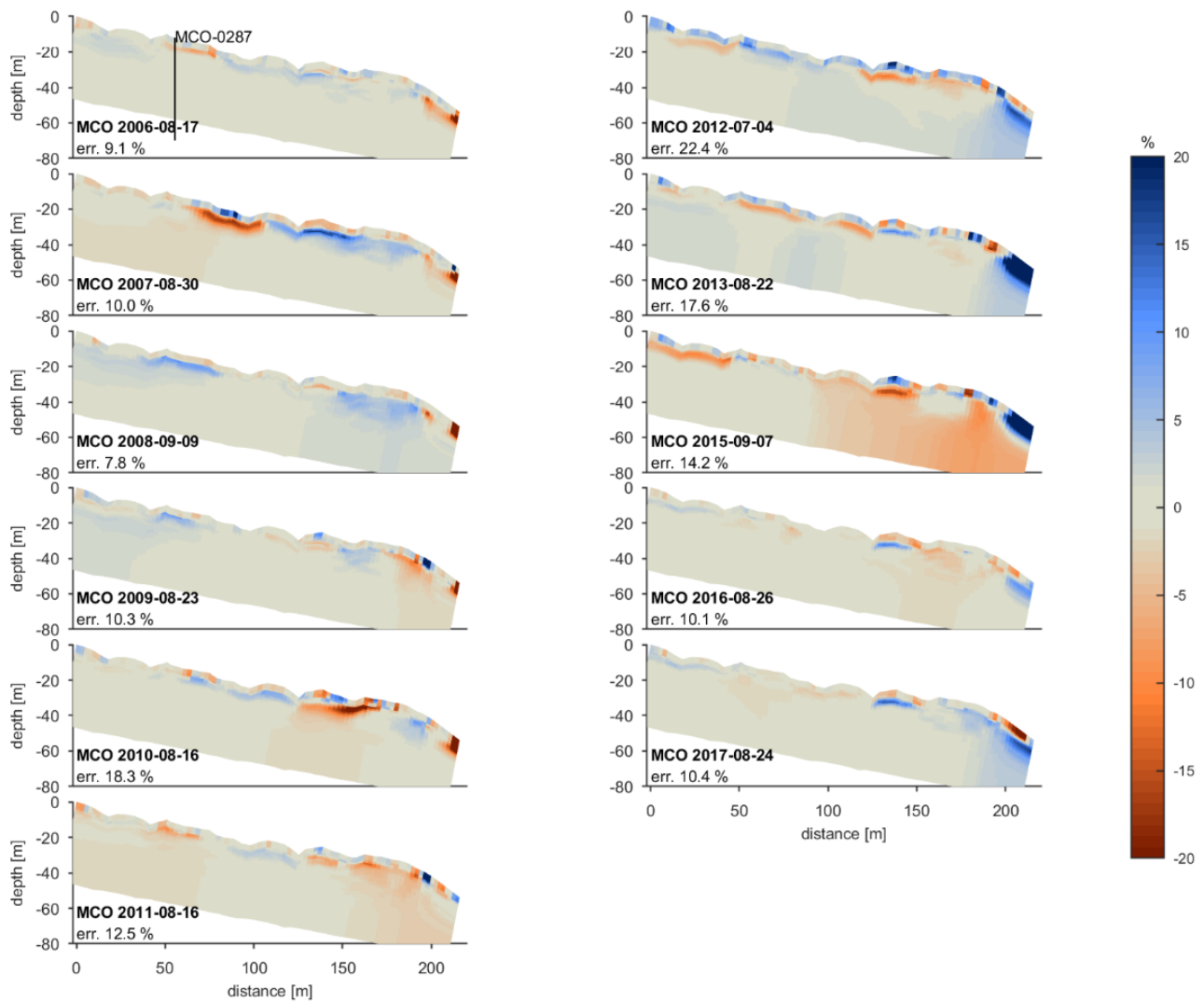
Figure S7. Percentage change of resistivity logarithm from the long-term median at MCO monitoring site. The strongest resistivity changes occur around 5-10 m depth. However, no obvious long-term trend is detectable at MCO, probably to the high ice content (reaching up to 80-100 %, Haeberli et al., 1998)
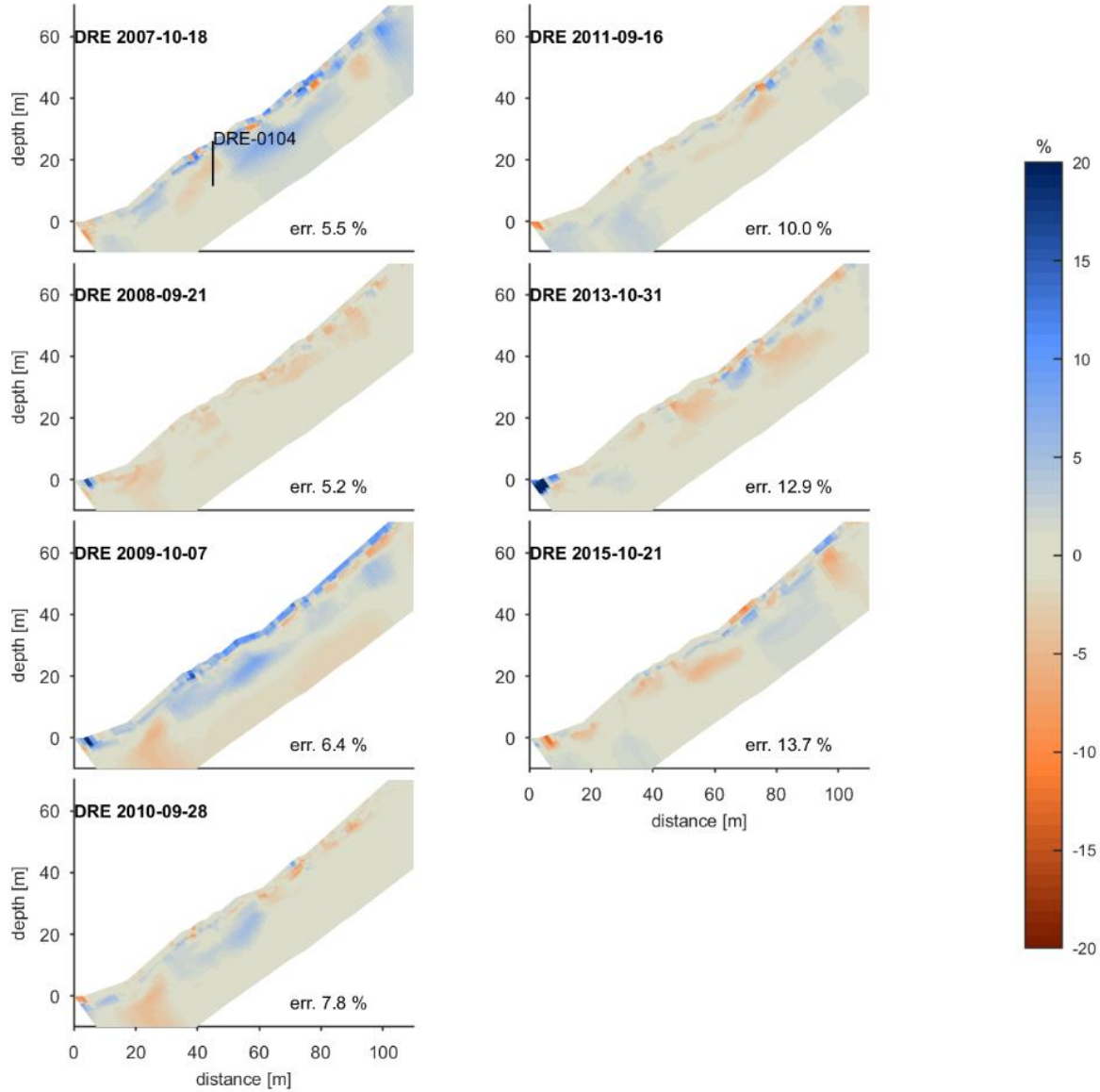
Figure S8. Percentage change of resistivity logarithm from the long-term median at DRE monitoring site for the year with comparable dates (mid-September to end of November). The spatial variability of the resistivity changes is rather high, probably to the complexity of air circulation processes.
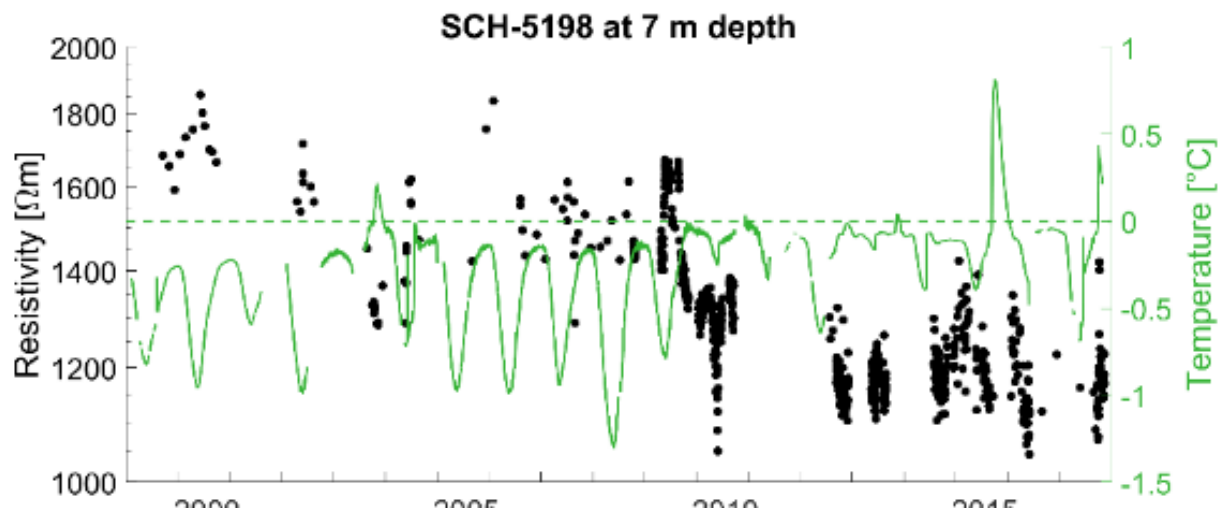
Figure S9. Resistivity and temperature comparison at same position (at borehole SCH-5198 at 7 m depth) at SCH monitoring site. Note the simultaneous resistivity decrease with temperature increase in 2003 and in 2009, when temperatures reach positive or near zero temperature. Since 2009, temperatures are higher in both winter and summer in comparison with the first decade of measurement (1999-2008), coinciding with remaining low resistivities. Temperatures reaching the melting point every year prevent the resistivity to recover values above 1400 Ωm. Therefore, the amount of liquid water remained high since 2009 in that part of the ground.
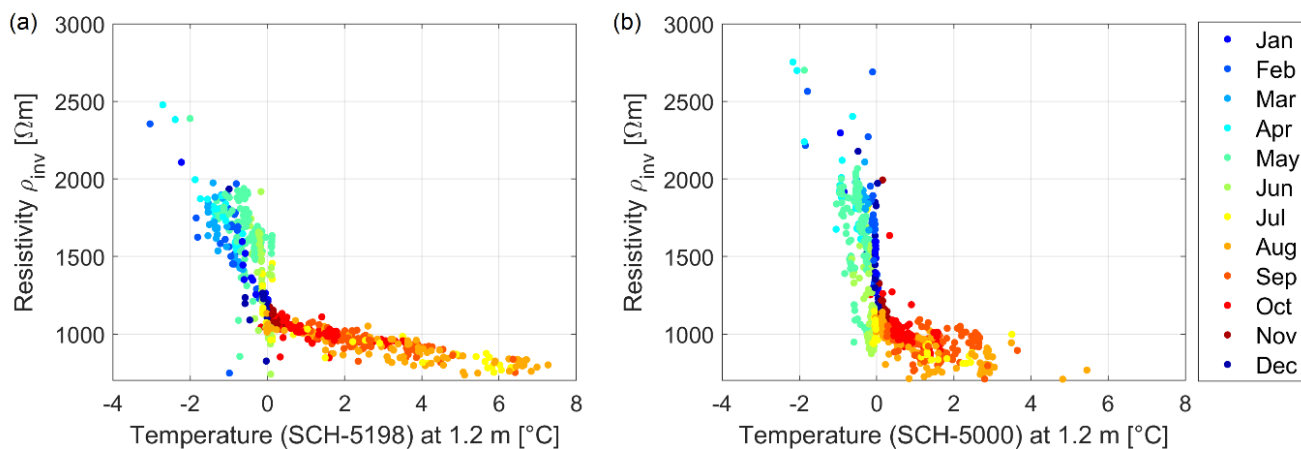
Figure S10. Scatter plots of resistivity against temperature at 1.2 m depth (a) at borehole SCH_5198 with a zero-curtain effect during the thawing period. (b) at borehole SCH_5000 with a zero curtain effect during the freezing period. Note that all pairs of data existing since 1999 are shown. Shallow surface (1.2 m depth) is highly influenced by annual variations. Note the contrary direction of the hysteresis loop at both boreholes at SCH monitoring site, probably due to local heterogeneity in soil physical properties (water saturation, water chemistry, porosity and pore connectivity).
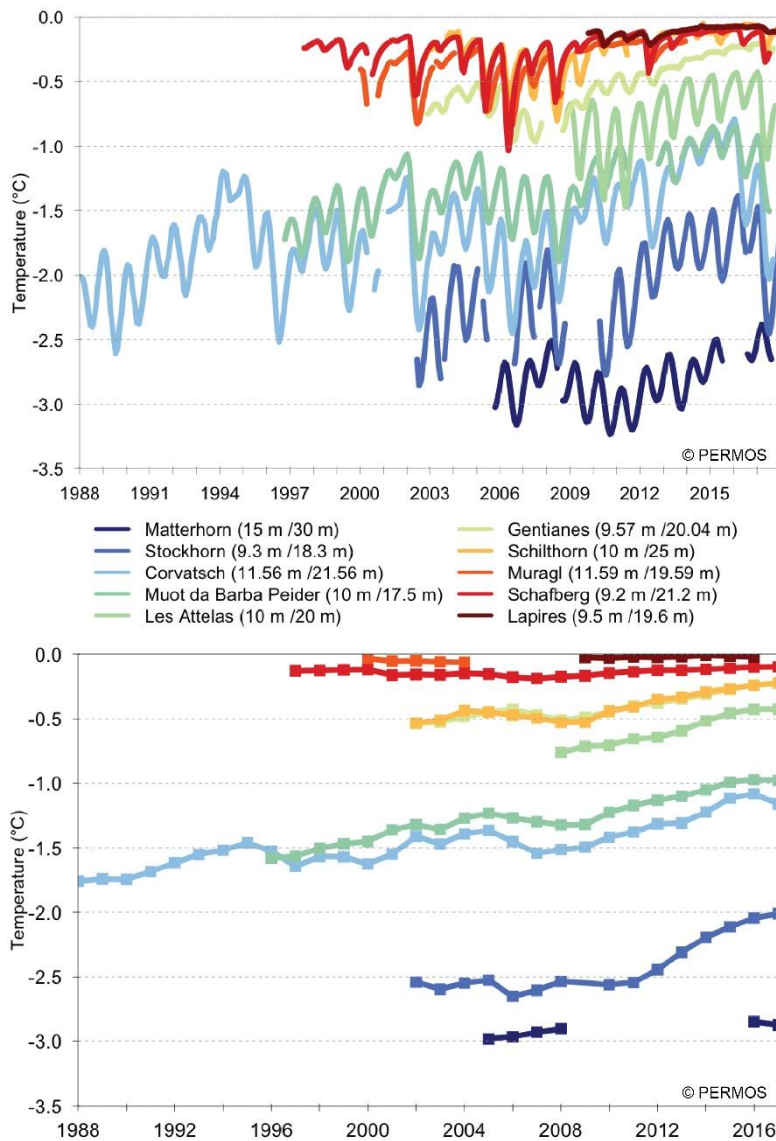
Figure S11.Standard PERMOS temperature plot (from PERMOS, 2016a) reproduction with permission.